Available online at www.sciencedirect.com
ScienceDirect
International Journal of Heat and Mass Transfer 50 (2007) 4229–4242
International Journal of HEAT and MASS TRANSFER
www.elsevier.com/locate/ijhmt

Combined mixed convection and radiation heat transfer in rectangular ducts rotating about a parallel axis

Han-Chieh Chiu [a], Jer-Huan Jang [a], Wei-Mon Yan [b,*]

[a] Department of Mechanical Engineering, Technology and Science Institute of Northern Taiwan, Beitou, Taipei 112, Taiwan, ROC
[b] Department of Mechatronic Engineering, Huafan University, Shih Ting, Taipei 223, Taiwan, ROC

Received 13 October 2006; received in revised form 16 February 2007
Available online 2 May 2007

Abstract

The study of combined heat transfer of convection and radiation in rectangular ducts rotating in a parallel mode was investigated numerically in detail. The coupled momentum and energy equations are solved by the DuFort–Frankel numerical scheme to examine the interactions of convection with radiation. The integro-differential radiative transfer equation is solved by the discrete ordinates method. Results are presented over a wide range of the governing parameters. The present results reveal that the rotational effect in a square duct is more significant than that in a rectangular one. The predictions also demonstrate that the radiation presents significant effects on the axial distributions of the total Nusselt number, Nu_t, and tends to reduce the centrifugal-buoyancy effects. The effect of rotation on the Nu_t is restricted in the entrance region, however, the radiation affects the heat transfer through out the channel. Additionally, the Nu_t increases with the decrease in the conduction-to-radiation parameter N_C.

Keywords: Convection; Rectangular ducts; Radiation; Rotating

1. Introduction

Combined heat transfer of convection and radiation in rotating ducts is of interest in many engineering applications, such as solar collectors, electronic equipments, heat exchangers and coolant passage for the cooling of turbine or rotor blades. The rotation induces additional body forces, i.e., centrifugal and Coriolis forces, acting on the flow, so that the momentum transfer mechanism becomes more complex. Separate calculation of convection and radiation effects without consideration of their interaction is used in many studies due to the weak radiation effect. However, as convection and radiation effects are both of the same importance, it would lead to significant errors in the results, because the presence of thermal radiation in the flow alters the temperature distributions. Hence, momentum, energy and radiation transport equations must be solved simultaneously in order to determine the local velocity, temperature and heat transfer rate, when radiation effect is considered.

As well known, the rotating channel flows have been extensively studied experimentally and numerically, in order to investigate the heat transfer and flow characteristics, as is evident in the study by Soong and Yan [1]. The first theoretical study of fully-developed convective heat transfer with rotating parallel ducts was by Morris [2] using the perturbation analysis. However, some studies are restricted in the effect of Coriolis force on the flow fields with unheated rotating ducts [3–10]. Some studies have been made of the flow and heat transfer in rotating ducts without the added complexity of centrifugal-buoyancy and thermal radiation [11–15].

Skiadaressis and Spalding [16] numerically investigated laminar mixed convection heat transfer and fluid flow in developing and fully-developed regions of a circular tube rotating in parallel mode. Mahadevappa et al. [17]

* Corresponding author. Tel.: +886 2 2663 2102; fax: +886 2 2663 1119.
E-mail address: wmyan@huafan.hfu.edu.tw (W.-M. Yan).

0017-9310/$ - see front matter © 2007 Elsevier Ltd. All rights reserved.
doi:10.1016/j.ijheatmasstransfer.2007.02.032

Nomenclature

a	height of rectangular duct (m)
b	width of rectangular duct (m)
D_e	hydraulic diameter, $2ab/(a+b)$ (m)
E	dimensionless eccentricity of the rotation ducts, H/D_e
f	friction factor, $2\bar{\tau}_W/(\rho u_0^2)$
G, G^*	dimensional and dimensionless incident radiation, $G^* = G/(4\bar{n}^2\sigma T_w^4)$
Gr_Ω	rotational Grashof number, $(\Omega^2 D_e)\beta(T_W - T_0)D_e^3/\nu^2$
H	radial distance from the axis of rotation to centerline of duct (m)
$\bar{h}$	circumferentially averaged heat transfer coefficient (W/m^2 °C)
J	rotational Reynolds number, $\Omega D_e^2/\nu$
k	thermal conductivity (W/m K)
m, m'	directions of the discrete ordinates
M, N	numbers of finite difference divisions in the Y and Z directions, respectively
n	direction of coordinate normal to the duct wall
$\bar{n}$	refractive index
N^*	order of the phase function
N_C	conduction-to-radiation parameter, $k\bar{\beta}/(4\bar{n}^2\sigma T_W^3)$
Nu_c	convective Nusselt number
Nu_r	radiative Nusselt number
Nu_t	total Nusselt number, $Nu_t = Nu_c + Nu_r$
Pe	Peclect number, $Pe = Re \cdot Pr$
$\bar{p}$, $\overline{P}$	dimensional and dimensionless cross-sectional mean pressure, respectively
P_n	Legendre polynomial
Pr	Prandtl number, ν/α
$\vec{q}_c$	convective heat flux
$\vec{q}_r$	radiation heat flux
$\vec{q}_t$	total heat flux
$\vec{Q}_r$	dimensionless radiation flux
Re	Reynolds number, $u_0 D_e/\nu$
R_0	rotational number, $\Omega D_e/u_0$
T	temperature (K)
T_0	inlet temperature (K)
T_w	wall temperature (K)
u, v, w	velocity components in the x, y and z directions, respectively (m/s)
U, V, W	dimensionless velocity components in the X, Y, Z directions, respectively
x, y, z	rectangular coordinate (m)
X, Y, Z	dimensionless rectangular coordinate, $X = x/(D_e \cdot Re)$, $Y = y/D_e$, $Z = z/D_e$
X^*	dimensionless axial coordinate, $X^* = X/Pr = x/(D_e \cdot Pe)$
∇^*	dimensionless gradient operator

Greek symbols

α	thermal diffusivity (m^2/s)
β	coefficient of thermal expansion
$\bar{\beta}$	extinction coefficient
γ	aspect ratio of a rectangular duct, a/b
ε_w	wall emissivity
θ	dimensionless temperature, T/T_W
θ_0	dimensionless inlet temperature ratio, T_0/T_W
η, μ, ζ	direction cosines
ν	kinematic viscosity (m^2/s)
ξ	dimensionless vorticity in axial direction
ρ	density (kg/m^3)
σ	Stefan–Boltzman constant
$\bar{\sigma}$	scattering coefficient
τ	optical thickness
τ_w	wall shear stress (kPa)
ψ	dimensionless radiation intensity $\pi I/(\bar{n}^2\sigma T_W^4)$
ϕ	scattering phase function
ω	single scattering albedo
$\vec{\Omega}$, $\vec{\Omega}'$	outward and inward direction of radiation
Ω	angular velocity of rotation

Subscripts

b	bulk fluid quantity
c	convective
0	condition at inlet
r	radiative
t	total
w	value at wall

Superscript

–	averaged value

analyzed fully-developed flow and heat transfer under influence of rotation-induced buoyancy in rotating rectangular and elliptical ducts. In experimental work on laminar [18,19] and turbulent [20,21] entrance flow in rotating ducts of parallel mode, it was found that the increase in the flow resistance due to rotation in the entrance region is typically 30–40% in the laminar flow regime, but 10% in the turbulent regime. Form the experiments on fully-developed laminar and turbulent flows in a rotating elliptical duct [22], the increase in heat transfer due to rotation for an elliptical duct lies between the values for circular and square ducts. Numerical and experimental studies on laminar flow of rectangular ducts for aspect ratio $\gamma = 0.5$ were conducted by Neti et al. [23] and Levy et al. [24], respectively. In their studies, the centrifugal-buoyancy effects on the flow and heat transfer characteristics were not addressed in detail. Recently, Tso et al. [25] and King and Wilson [26] numerically studied the effects of Coriolis force and buoyancy force on the flow with rotation. However, consideration of thermal radiation is not included in their investigations.

As far as combined convection and radiation are concerned, convection heat transfer in a stationary duct with radiation effect only (i.e., without thermal buoyancy) has been examined by several investigators during the past 30 years for ducts subjected to prescribed heat flux or wall temperature at the wall surfaces. Chawla and Chan [27] solved the problem of thermally developing Poiseuille flow with scattering using the method of collocation with splines. The combined convection and radiation heat transfer in thermally developing pipe flow was examined by Azad and Modest [28]. In their work, a modified differential approximation method was used to solve the radiative transport, accounting diffuse reflection and linear anisotropic scattering effects. Yender and Ozisik [29] investigated the combined convection and radiation heat transfer for absorbing, emitting, and isotropic-scattering gray turbulent fluid flow in parallel-plate channel. A similar investigation was also done by Krishnapradas et al. [30].

According to the literature survey, it is noted that the combined convection and radiation heat transfer in rectangular ducts rotating about a parallel axis has not been well evaluated. This motivates the present study, which treats the mixed convection heat transfer in rotating rectangular ducts with consideration of thermal radiation effects.

2. Analysis

Fig. 1 shows a rectangular duct of height a and width b rotating at a constant angular speed Ω around an axis parallel to the duct itself. The distance of the duct centerline to the rotating axis is the eccentricity H. The flow enters the duct inlet ($x = 0$) with a uniform axial velocity u_0 and uniform temperature T_0. Variables u, v, and w are the velocity components in the x, y, and z directions, respectively. In order to simplify the analysis, the flow is assumed to be steady and incompressible. Additionally, the participating gas is assumed to be gray, absorbing, emitting, and scattering. The Boussinesq approximation is invoked to account for the centrifugal-buoyancy effects.

For a sufficiently fast rotating system, gravitational force is neglected for its small magnitude compared to the centrifugal force. Axial diffusion in momentum and energy balance is also ignored for small influences. This is justified as the Peclect number Pe is high enough, e.g. $Pe > 100$ [31].

According to the above assumptions, the problem can be formulated by the following dimensionless vorticity-velocity formulations:

Table 1
The discrete directions and quadrature weights for the S_6 method (one octant only)

m	μ_m	η_m	ζ_m	w_m^*
1	0.948235	0.224556	0.224556	$\pi/6$
2	0.689048	0.689048	0.224556	$\pi/6$
3	0.224556	0.948235	0.224556	$\pi/6$
4	0.689048	0.224556	0.689048	$\pi/6$
5	0.224556	0.689048	0.689048	$\pi/6$
6	0.224556	0.224556	0.948235	$\pi/6$

Table 2
Comparison of local Nu_t for various grid arrangement for $\gamma = 1$, $J = 600$, $Gr_\Omega = 2 \times 10^4$, $N_C = 0.1$, $\tau = 1$, $\omega = 0$ and $\varepsilon_w = 0.5$

$M \times N(\Delta X^*)$	X^*					
	0.001	0.005	0.01	0.05	0.1	0.3
$51 \times 51(1 \times 10^{-6}$–$1.5 \times 10^{-4})$	13.93	7.54	6.31	6.84	6.54	5.93
$81 \times 81(1 \times 10^{-6}$–$1.5 \times 10^{-4})$	13.63	7.52	6.31	6.80	6.54	5.93
$51 \times 51(1 \times 10^{-7}$–$1.5 \times 10^{-4})$	13.88	7.52	6.29	6.84	6.54	5.93
$31 \times 31(1 \times 10^{-6}$–$1.5 \times 10^{-4})$	15.65	7.60	6.30	6.84	6.57	5.93

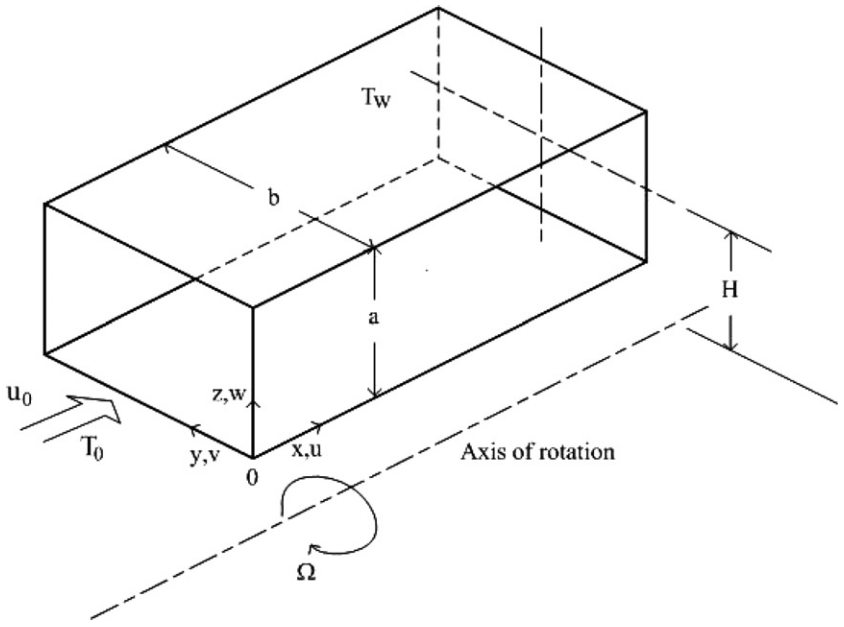

Fig. 1. Schematic diagram of the physical system.

$$U\frac{\partial U}{\partial X}+V\frac{\partial U}{\partial Y}+W\frac{\partial U}{\partial Z}=-\frac{\mathrm{d}\overline{P}}{\mathrm{d}X}+\frac{\partial^2 U}{\partial Y^2}+\frac{\partial^2 U}{\partial Z^2} \tag{1}$$

$$\frac{\partial^2 V}{\partial Y^2}+\frac{\partial^2 V}{\partial Z^2}=-\frac{\partial \xi}{\partial Z}-\frac{\partial^2 U}{\partial X\partial Y} \tag{2}$$

$$\frac{\partial^2 W}{\partial Y^2}+\frac{\partial^2 W}{\partial Z^2}=\frac{\partial \xi}{\partial Y}-\frac{\partial^2 U}{\partial X\partial Z} \tag{3}$$

$$\begin{aligned}U\frac{\partial \xi}{\partial X}+V\frac{\partial \xi}{\partial Y}+W\frac{\partial \xi}{\partial Z}+\xi\frac{\partial U}{\partial X}+\left(\frac{\partial U}{\partial Y}\cdot\frac{\partial W}{\partial X}-\frac{\partial U}{\partial Z}\cdot\frac{\partial V}{\partial X}\right)\\ =\frac{\partial^2 \xi}{\partial Y^2}+\frac{\partial^2 \xi}{\partial Z^2}+2J\frac{\partial U}{\partial X}+\left(\frac{Y}{E}+1-\frac{1+\gamma}{4\gamma E}\right)\frac{Gr_\Omega}{1-\theta_0}\frac{\partial \theta}{\partial Z}\\ -\left(\frac{Z}{E}-\frac{1+\gamma}{4E}\right)\frac{Gr_\Omega}{1-\theta_0}\frac{\partial \theta}{\partial Y}\end{aligned} \tag{4}$$

$$\begin{aligned}U\frac{\partial \theta}{\partial X}+V\frac{\partial \theta}{\partial Y}+W\frac{\partial \theta}{\partial Z}\\ =\frac{1}{Pr}\left[\frac{\partial^2 \theta}{\partial Y^2}+\frac{\partial^2 \theta}{\partial Z^2}+\frac{(1-\omega)\tau^2}{N_C}(G^*-\theta^4)\right]\end{aligned} \tag{5}$$

where the dimensionless variables and groups are defined as follows:

$$\begin{aligned}&X=x/(D_eR_0);\quad Y=y/D_e;\quad Z=z/D_e;\quad U=u/u_0;\\ &V=vD_e/v;\quad W=wD_e/v;\quad \overline{P}=\bar{p}/(\rho u_0^2);\quad X^*=X/Pr;\\ &\theta=T/T_W;\quad Pr=v/\alpha;\quad \tau=\bar{\beta}D_e;\quad \omega=\bar{\sigma}/\bar{\beta};\\ &R_0=\Omega D_e/u_0;\quad J=\Omega D_e^2/v;\quad E=H/D_e;\quad N_C=k\bar{\beta}/(4\bar{n}^2\sigma T_W^3);\\ &Gr_\Omega=(\Omega^2 D_e)\beta(T_W-T_0)D_e^3/v^2;\\ &G^*=G/(4\bar{n}^2\sigma T_W^4);\quad \theta_0=T_0/T_W\end{aligned} \tag{6}$$

For proper calculation of the axial pressure gradient, $-\mathrm{d}\overline{P}/\mathrm{d}X$, the global mass conservation has to be satisfied at each axial location. Hence

$$\int_0^{(1+\gamma)/(2\gamma)}\int_0^{(1+\gamma)/2} U\,\mathrm{d}Y\,\mathrm{d}Z=\frac{(1+\gamma)^2}{(4\gamma)} \tag{7}$$

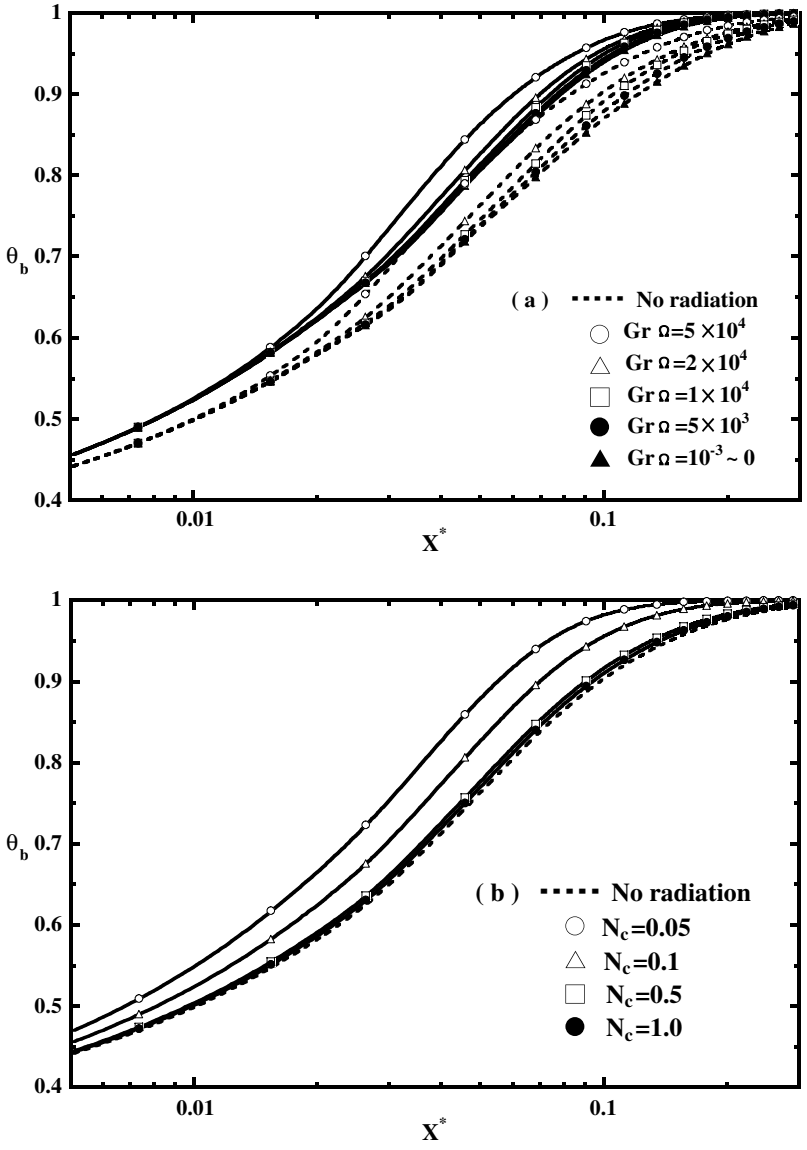

Fig. 2. Effects of Gr_Ω and N_C on the axial distributions of bulk temperature.

The boundary conditions for the convective governing equations of this problem are given by

at walls: $U = V = W = 0, \quad \theta = 1$ (8)

at entrance: $U = 1, \quad V = W = \xi = 0, \quad \theta = \theta_0$ (9)

In Eq. (5), G^* is the dimensionless incident radiation function evaluated from the radiation intensity condition, which is defined as

$$G^* = \frac{G}{4\bar{n}^2\sigma T_W^4} = \frac{1}{4\pi}\int_{\vec{\Omega}=4\pi}\psi\,\mathrm{d}\vec{\Omega} \tag{10}$$

The dimensionless intensity of radiation $\psi = \pi I/(\bar{n}^2\sigma T_W^4)$ in the direction $\vec{\Omega}$ can be evaluated from the solution of radiation transport equation (RTE).

$$\eta\frac{\partial\psi}{\partial Y} + \mu\frac{\partial\psi}{\partial Z} + \tau\psi = (1-\omega)\tau\theta^4 + \frac{\omega\tau}{4\pi}\int_{\Omega'=4\pi}\phi(\vec{\Omega}',\vec{\Omega})\psi\,\mathrm{d}\Omega' \tag{11}$$

Once the dimensionless radiation intensity ψ is known, the dimensionless radiation flux vector and incident radiation are determined from their definitions as

$$\vec{Q}_r = \frac{\vec{q}_r}{4\bar{n}^2\sigma T_W^4} = \frac{1}{4\pi}\int_{\vec{\Omega}=4\pi}\vec{\Omega}\psi\,\mathrm{d}\vec{\Omega} \tag{12}$$

Following the usual definition, the peripheral average of friction parameter, fRe, can be expressed based on the axial velocity gradient on the duct walls, viz.

$$fRe = -2(\overline{\partial U/\partial n})_w \tag{13}$$

The total wall heat flux, which is the sum of the convective and radiative contributions, can be expressed in terms of a local total Nusselt number Nu_t

$$Nu_t = Nu_C + Nu_r = \frac{\overline{\partial\theta_W/\partial n}}{1-\theta_b} + \frac{\tau\overline{Q}_r/N_C}{1-\theta_b} \tag{14}$$

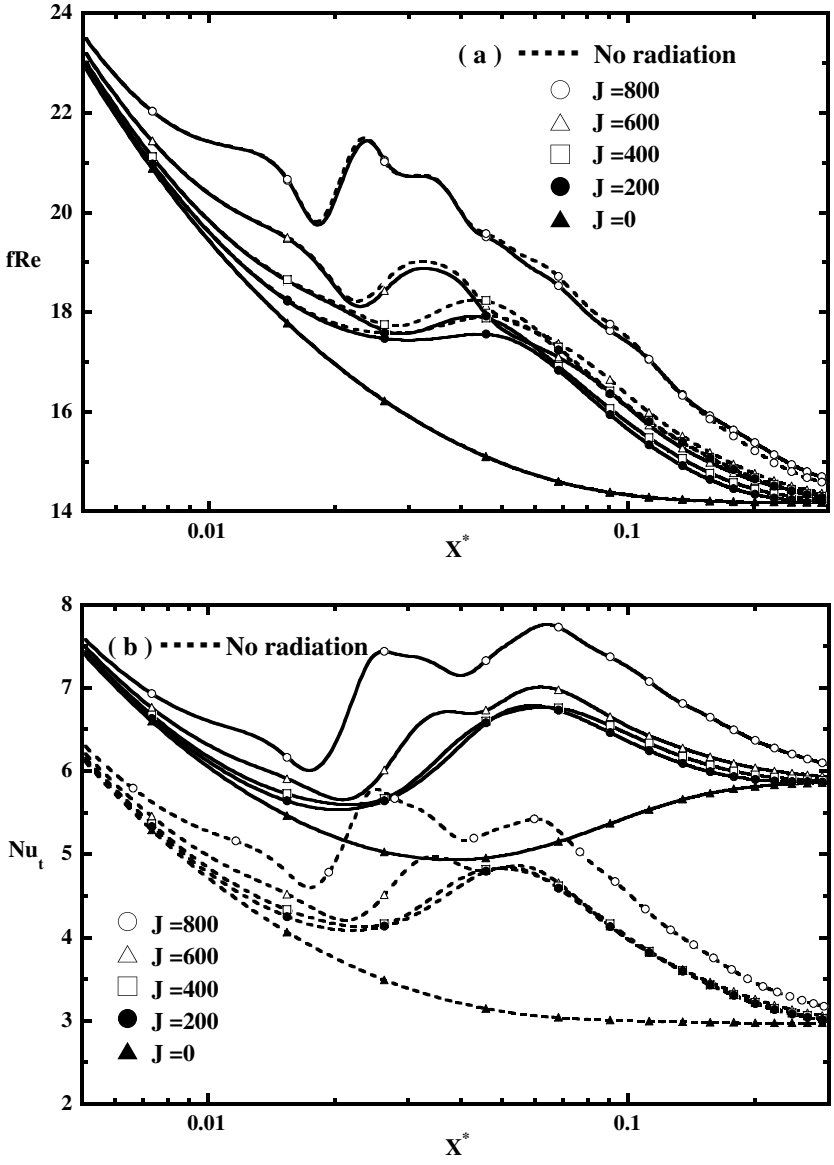

Fig. 3. Effects of J on the axial distributions of fRe and Nu_t.

where Nu_C and Nu_r denote the local convective Nusselt number and radiative Nusselt number, respectively. Here the overbar means the average around the perimeters.

The solutions depends on two geometry parameters, γ and E, three flow/thermal parameters, J, Gr_Ω, and Pr, and five radiation/convection parameters, N_C, τ, ω, ε_w, and θ_0. The rotational Reynolds number J characterizes the Coriolis force effect or a measure of the relative strength of Coriolis force to viscous force. The value of Gr_Ω measures the significance of the rotation-induced buoyancy effect. The conduction-to-radiation parameter N_C characterizes the relative importance of conduction with respect to radiation. The effect of radiation is getting strong as the N_C decreases. To reduce the computational efforts, the parameters, Pr, E, and θ_0 are fixed to be 0.7, 10, and 0.3, respectively. Effects of the rest parameters are studied in detail.

3. Solution method

In this study, the governing equations are solved by the vorticity-velocity method for three-dimensional parabolic flow [32]. The equations for the unknowns U, V, W, ξ, θ and $d\overline{P}/dX$ are coupled. A numerical finite-difference scheme based on the vorticity-velocity method is used to obtain the solution of Eqs. (1)–(5). Details of the solution procedures have been described elsewhere [33], and are not repeated here. The solution to the radiative transfer equation is obtained by the S_N or the discrete ordinates method [34–36]. In this approach, the solid angle 4π is discretized into a finite number of directions. The discrete ordinates form of the radiative transport equation can be obtained by evaluating equation at each of the discrete directions and by replacing the integral term by a numerical quadrature to give

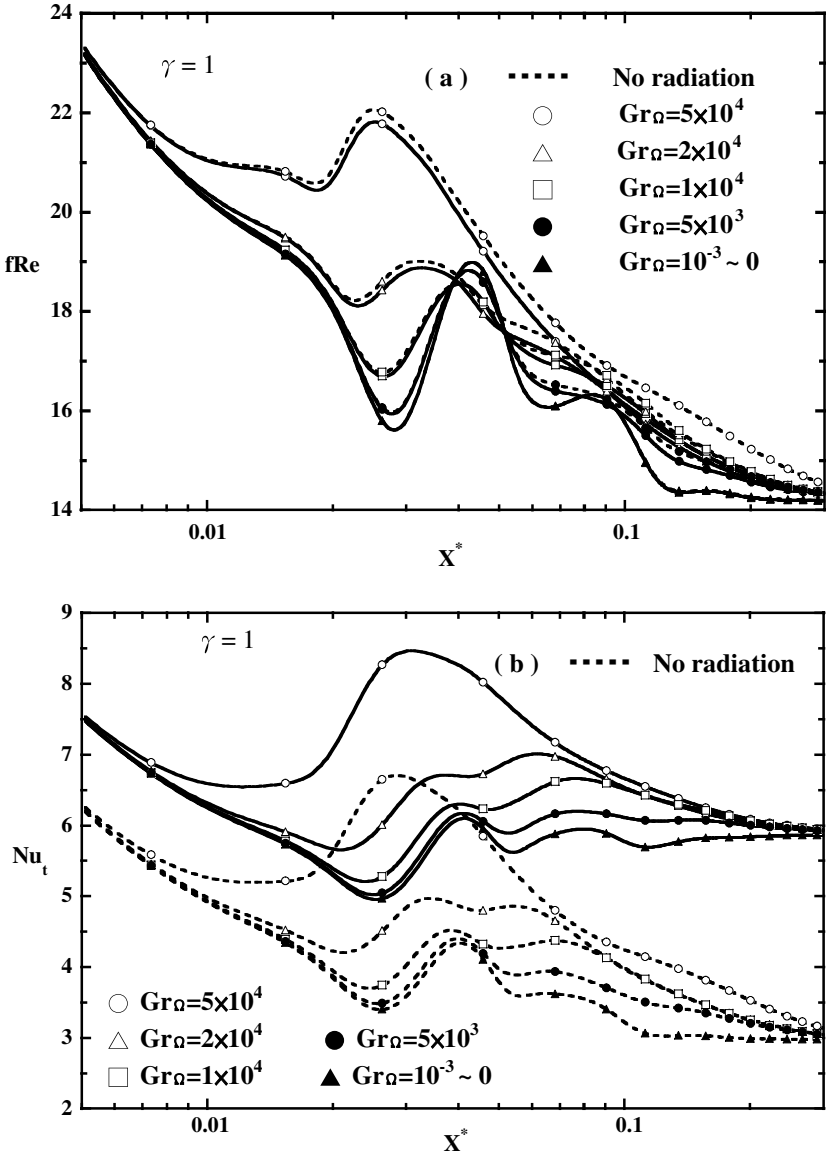

Fig. 4. Effects of Gr_Ω on the axial distributions of fRe and Nu_t for $\gamma = 1$.

$$\eta_m \frac{\partial \psi_m}{\partial Y} + \mu_m \frac{\partial \psi_m}{\partial Z} + \tau \psi_m = (1-\omega)\tau\theta^4 + \frac{\omega\tau}{4\pi} \sum_{m'} w^*_{m'} \phi_{m'm} \psi_{m'} \tag{15}$$

with the boundary conditions,

$$\psi_m = \varepsilon_W + \frac{(1-\varepsilon_W)}{\pi} \sum_{m'} \psi_{m'} |\eta_{m'}| w^*_{m'};$$
$$\eta_m > 0, \quad \eta_{m'} < 0, \quad Y = 0 \tag{16a}$$

$$\psi_m = \varepsilon_W + \frac{(1-\varepsilon_W)}{\pi} \sum_{m'} \psi_{m'} |\eta_{m'}| w^*_{m'};$$
$$\eta_m < 0, \quad \eta_{m'} > 0, \quad Y = (1+\gamma)/(2\gamma) \tag{16b}$$

$$\psi_m = \varepsilon_W + \frac{(1-\varepsilon_W)}{\pi} \sum_{m'} \psi_{m'} |\eta_{m'}| w^*_{m'};$$
$$\mu_m > 0, \quad \mu_{m'} < 0, \quad Z = 0 \tag{16c}$$

$$\psi_m = \varepsilon_W + \frac{(1-\varepsilon_W)}{\pi} \sum_{m'} \psi_{m'} |\eta_{m'}| w^*_{m'};$$
$$\mu_m < 0, \quad \mu_{m'} > 0, \quad Z = (1+\gamma)/2 \tag{16d}$$

where subscript m and m' represent the direction of the discrete ordinates, and $w^*_{m'}$ are the quadrature weights. The discrete form of the phase function $\phi_{m'm}$ is given by

$$\phi_{m'm} = \sum_{n=0}^{N^*} a_n P_n(\zeta_{m'}\zeta_m + \eta_{m'}\eta_m + \mu_{m'}\mu_m) \tag{17}$$

The accuracy of the S_N method depends on the choice of the quadrature scheme. In this work, the momentum-matching technique suggested by Carson and Lathrop [37] is applied to calculate the discrete directions and quadrature weights as listed in Table 1. The total number of the

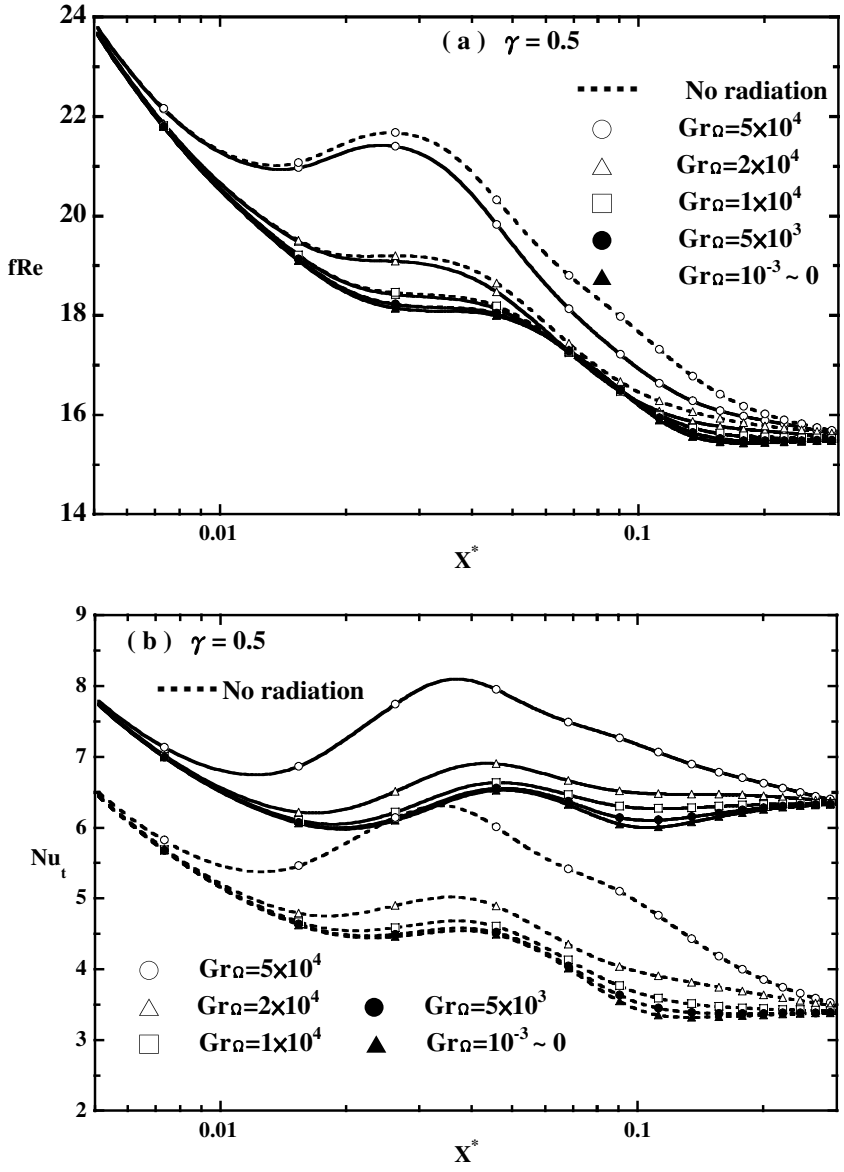

Fig. 5. Effects of Gr_Ω on the axial distributions of fRe and Nu_t for $\gamma = 0.5$.

discrete directions is 24 when the S_6 scheme is used for a two-dimensional geometry. Eqs. (15), (16a)–(16d), (17) are solved using the procedure described by Modest [36] to calculate the dimensionless radiation intensity, radiation flux, and incident radiation.

To examine the grid dependence of the numerical results, a numerical experiment was performed with various grid distributions in cross-section plane ($M \times N$) and axial step size (ΔX^*). In this work, grids were uniformly arranged in the cross plane but non-uniform in the axial direction to account for the uneven variations of velocity and temperature in the entrance region. It was found from the Table 2 that the deviations in local total Nusselt number Nu_t calculated with $M \times N = 51 \times 51$ and 71×71 $\Delta X^* = 1 \times 10^{-6}$–$1.5 \times 10^{-4}$ are always less than 2% for typical case with $\gamma = 1$, $J = 600$, $Gr_\Omega = 2 \times 10^4$, $N_C = 0.1$, $\tau = 1$, $\omega = 0$ and $\varepsilon_w = 0.5$. Furthermore, the deviations in Nu_t calculated using $M \times N(\Delta X^*) = 51 \times 51(\Delta X^* = 1 \times 10^{-6}$–$1.5 \times 10^{-4})$ and $51 \times 51(\Delta X^* = 1 \times 10^{-7}$–$1.5 \times 10^{-4})$ are all less than 2%. Accordingly, the computations involving a $M \times N(\Delta X^*) = 51 \times 51(\Delta X^* = 1 \times 10^{-6}$–$1.5 \times 10^{-4})$ grid are considered to be sufficiently accurate to describe the fluid flow and heat transfer in a square duct rotating in a parallel mode. As for the grids employed for the rectangular ducts various aspect ratio cases, the 81×41 or 41×81 grid arrangement was used for aspect ratio $\gamma = 2$ or 0.5, respectively. As a partial verification of the computational procedure, results were initially obtained for convection heat transfer in a rotating square duct without thermal radiation effect. The results for heat transfer and friction factor were compared with those of Soong and Yan [1]. The predicted Nusselt number and friction factor were found to agree with those of Soong and Yan [1] within 2%.

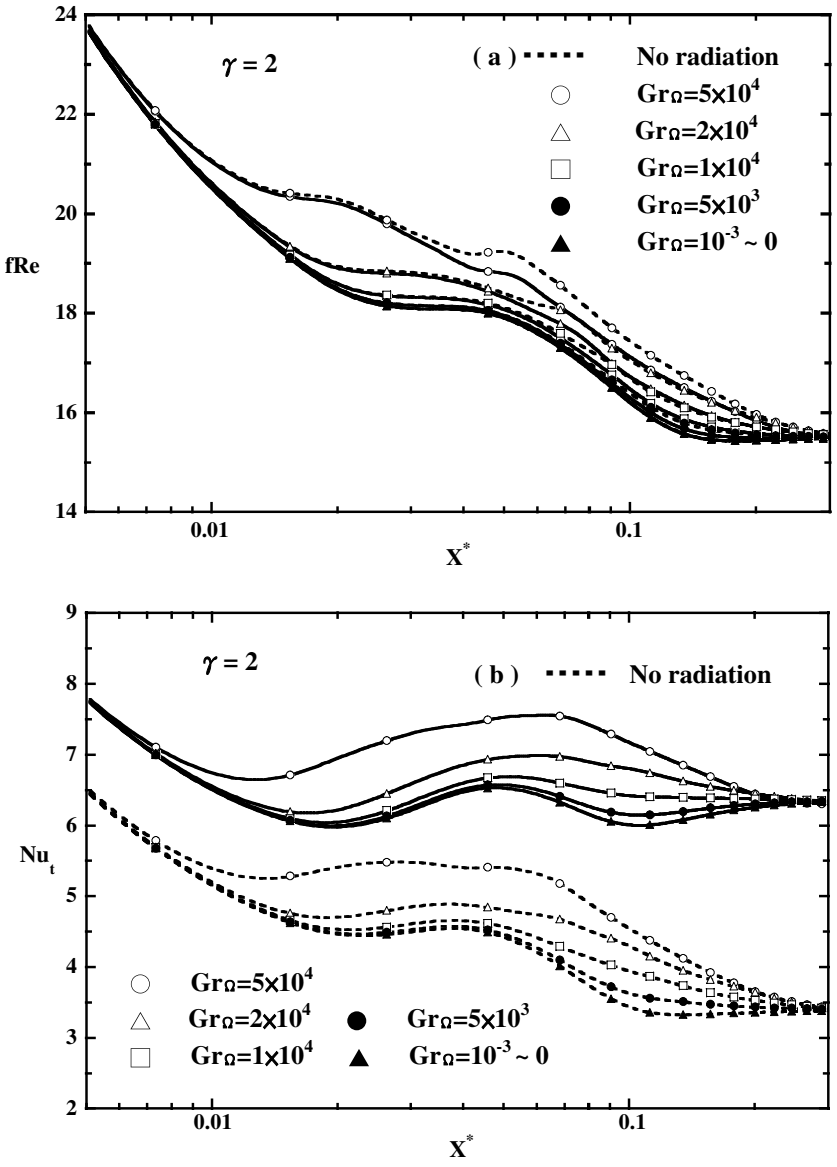

Fig. 6. Effects of Gr_Ω on the axial distributions of fRe and Nu_t for $\gamma = 2$.

4. Results and discussion

For practical applications, the bulk temperature of the fluid along the channel is important. Fig. 2 shows the effects of rotational Grashof number Gr_Ω and conduction-to-radiation parameter N_C on the axial distributions of the normalized bulk temperature θ_b. It is clearly seen from Fig. 2a that the value of θ_b rises fast in the entrance region and converges to unity. The thermal development (temperature rise) is enhanced with increased Gr_Ω and is reduced by radiation effect. The magnitude of Gr_Ω indicates the influence of centrifugal buoyancy on the fluid flow. Therefore, the centrifugal buoyancy increases the thermal development along the duct. Also, it is seen that the effect of radiation is greater than that without radiation. It can be easily found in Fig. 2b that the bulk temperature develops quickly with smaller N_C. Similar to the curves in Fig. 2a, the effect is restricted in the entrance region. Beyond this region, the bulk temperature is not influenced by either buoyancy or radiation. In addition, the bulk temperature is almost the same as that without radiation when N_C is large ($N_C > 0.5$), which corresponds to a weak radiation–convection interaction. It can be easily realized that the bulk temperature is higher with stronger radiation effect ($N_C = 0.05$) due to radiative heat flux being an additional mode of energy transport.

The axial distributions of fRe and Nu_t for different rotational Reynolds numbers with and without radiation effect are depicted in Fig. 3. Both the values of fRe and Nu_t monotonically decline along the axial location without rotation and radiation effects. Rotation induces the secondary flow and vorticity and in turn causes raise and fluctuation of fRe and Nu_t. Near the very inlet, both fRe and Nu_t are not significantly influenced by rotation. The rotational

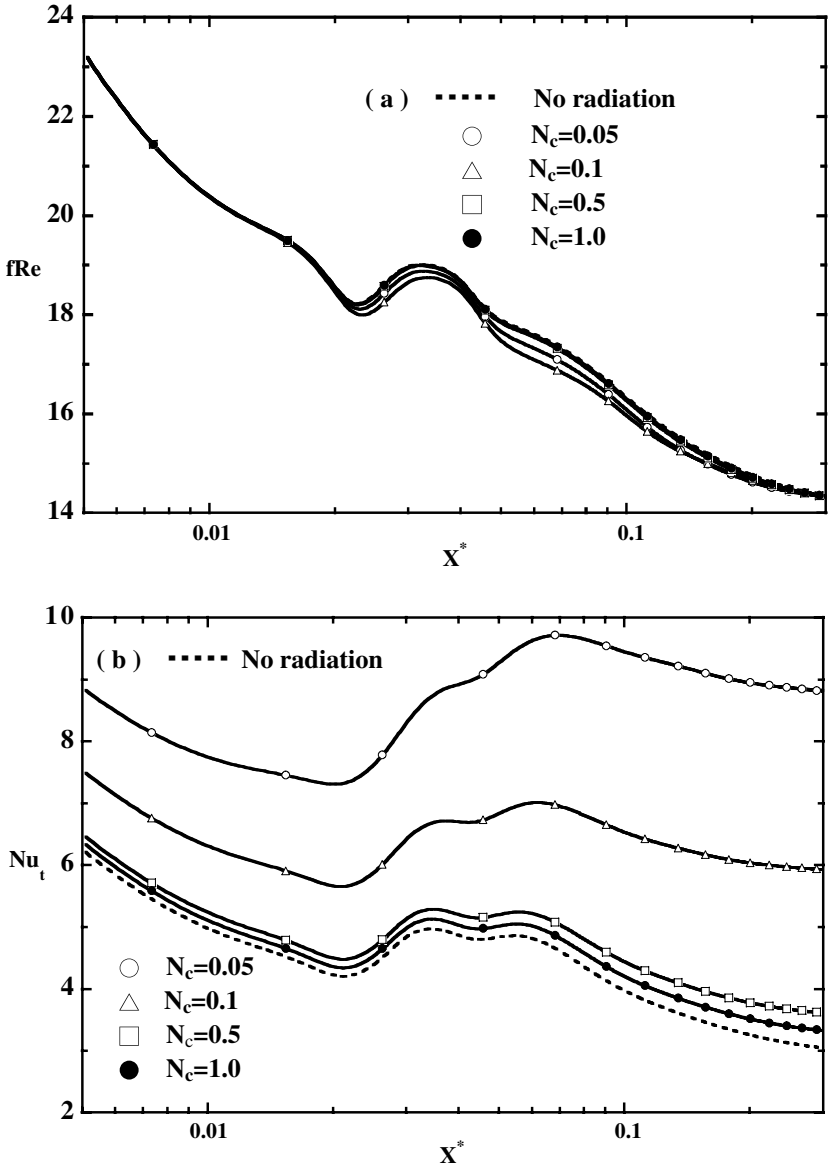

Fig. 7. Effect of N_C on the axial distributions of fRe and Nu_t.

effect then axially increases and causes a local minimum fRe (Nu_t). The values are raised with increasing rotational speed (Reynolds number) due to the stronger Coriolis force. For $J = 600$ or higher, oscillations in the variations of fRe and Nu_t exist after the first local minimum. This behavior is related to the emergence and decay of the second pair of vortices. It is observed that the radiation has weak influence on the variation of fRe, but it strongly raises the value of Nu_t, from the very inlet to the farther downstream region. This influence is axially augmented. With or without radiation effect, the curves asymptotically converge and temperature fields approach the fully-developed conditions.

Figs. 4–6 show the effect of rotational Grashof number Gr_Ω on the local friction factor fRe and total Nusselt number, with different aspect ratio γ. Fig. 4 present the axial distribution of fRe and Nu_t with different Gr_Ω for a square duct ($\gamma = 1.0$). It is clear that both fRe and Nu_t are raised with increasing Gr_Ω. Similar to the curves in Fig. 3, oscillations in the variations of fRe and Nu_t exist after the first local minimum for $Gr_\Omega \leqslant \times 10^4$. The observation of the curves also reveals that the deviations due to buoyancy take place in the entrance region. However, the influence of radiation on Nu_t extends to the downstream. It is clear that the Nu_t curves with and without radiation show different convergence values. Although radiation significantly raises the curves of Gr_Ω, it does not affect their features and the locations where the local minimal take place. Besides, the centrifugal-buoyancy effect can be neglected for $Gr_\Omega \leqslant \times 10^3$ [14].

Fig. 5 show the curves of the same conditions as that in Fig. 4, except for $\gamma = 0.5$. It is found that the curves present similar trends, but they are more smooth than those of a square duct ($\gamma = 1.0$). It is seen in Fig. 5a that the local

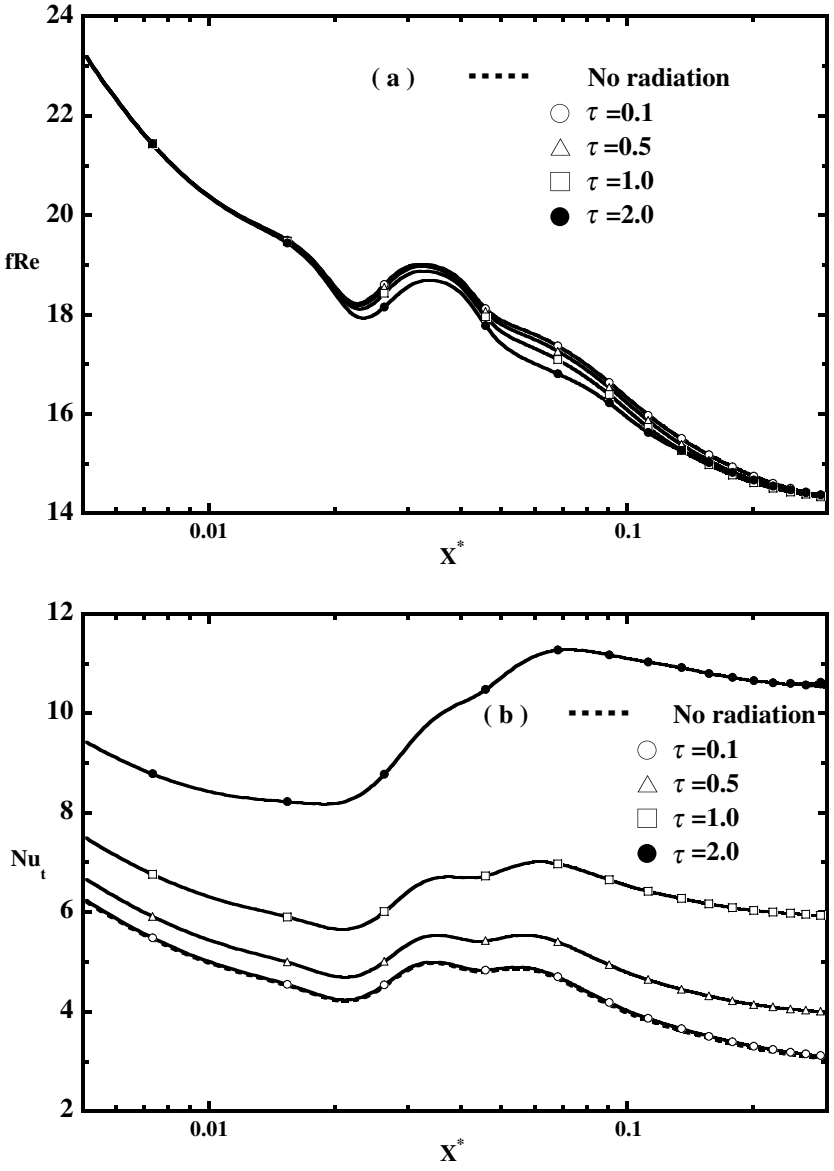

Fig. 8. Effect of τ on the axial distributions of fRe and Nu_t.

minimum does not exist for $Gr_\Omega \leqslant \times 10^4$, meaning the buoyancy effect on fRe (Nu_t) is weaker than that of square duct. It is also observed that the radiation still shows insignificant effect on fRe and significant effect on Nu_t. The axial distribution of fRe and Nu_t for the same conditions of Fig. 4 is shown in Fig. 6, except for $\gamma = 2.0$. These curves have similar features with less deviation and less fluctuation, suggesting even weaker buoyancy effect. The fRe curves monotonically decline along the axial location. Although the value of γ influences fRe and Nu_t, the convergence values are seemingly unchanged. This suggests that the effect of geometry is restricted in the entrance region as well. Overall inspection of Figs. 4–6 indicates that the buoyancy effects are stronger for a square duct.

The effects of conduction-to-radiation parameter N_C on the axial distribution of fRe and Nu_t are presented in Fig. 7. In the very inlet region, the flow is dominated by convection, and the local fRe shows almost no deviation. As the flow proceeds downstream, the radiation begins to reduce fRe. Even though, it is seen in Fig. 7a that N_C only slightly reduces the local friction factor. For $N_C = 0.05$, the deviation of fRe is still insignificant. Contrarily, the value of Nu_t is strongly increased with decreasing N_C and the radiation effect dominates through out the channel. For $N_C \leqslant 1.0$, the value of Nu_t is significantly raised. This is due to two effects. The first is that radiation is additional mechanism for heat transfer through the fluid resulting in an increased heat flux. Secondly, the radiation source term augments the rate of thermal developments so that the bulk temperature approaches the wall temperature at a more rapid rate. Both effects act to increase the local total Nusselt number Nu_t. Near the inlet, Nu_t is raised only by the additional radiative

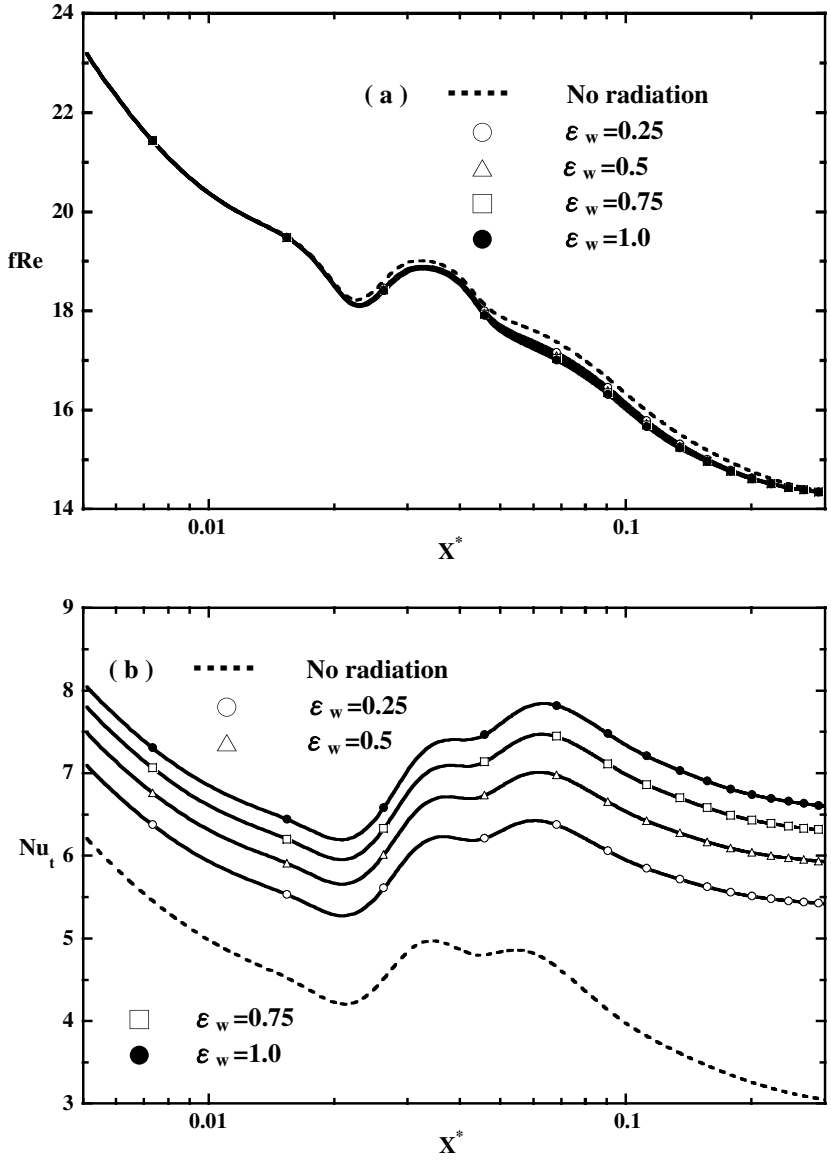

Fig. 9. Effect of ε_w on the axial distributions of fRe and Nu_t.

heat flux, while further downstream, the more rapid thermal development contributes when the bulk temperature approaches the wall temperature.

Fig. 8 show the effect of optical thickness on the axial distribution of fRe and Nu_t. In Fig. 8a, it is seen that the curves are very close. It means the local friction factor is not significantly affected by optical thickness. Even for $\tau = 2.0$, the local friction factor is slightly reduced. Besides, the influence only takes place in the entrance region. However, it does show the trend that the friction factor decreases with increased optical thickness. In contrast, the data in Fig. 8b show that optical thickness influences the value of Nu_t through out the channel. A strong radiatively participating medium corresponds to a larger optical thickness. It is easy to see that there is more heat released from such a medium than from a weak radiatively participating medium. Thus the value of Nu_t is increased with an increase in τ. Comparison of the curves suggests that increasing optical thickness not only increases value of Nu_t, but also axially augments the effect.

The effect of wall emissivity ε_w on the axial distribution of fRe and Nu_t is depicted in Fig. 9. Similarly, it is found that the effect of ε_W on fRe is weak, even weaker than the effect of optical thickness, meaning that the value of fRe is almost emissivity independent. Fig. 7b shows the influence of ε_w on Nu_t. The value of Nu_t is raised with increasing ε_w. Compared with the influence of τ, increasing emissivity does not show an augmented effect of radiation. Contrarily, it shows a saturation of effect at high value. The heat transfer is the maximum for a black duck ($\varepsilon_w = 1.0$)

In many applications, scattering processes are important in radiative heat transfer if particulates are present in the fluid. Therefore, the effects of the single scattering albedo on the fluid flow and heat transfer are of interest. For illus-

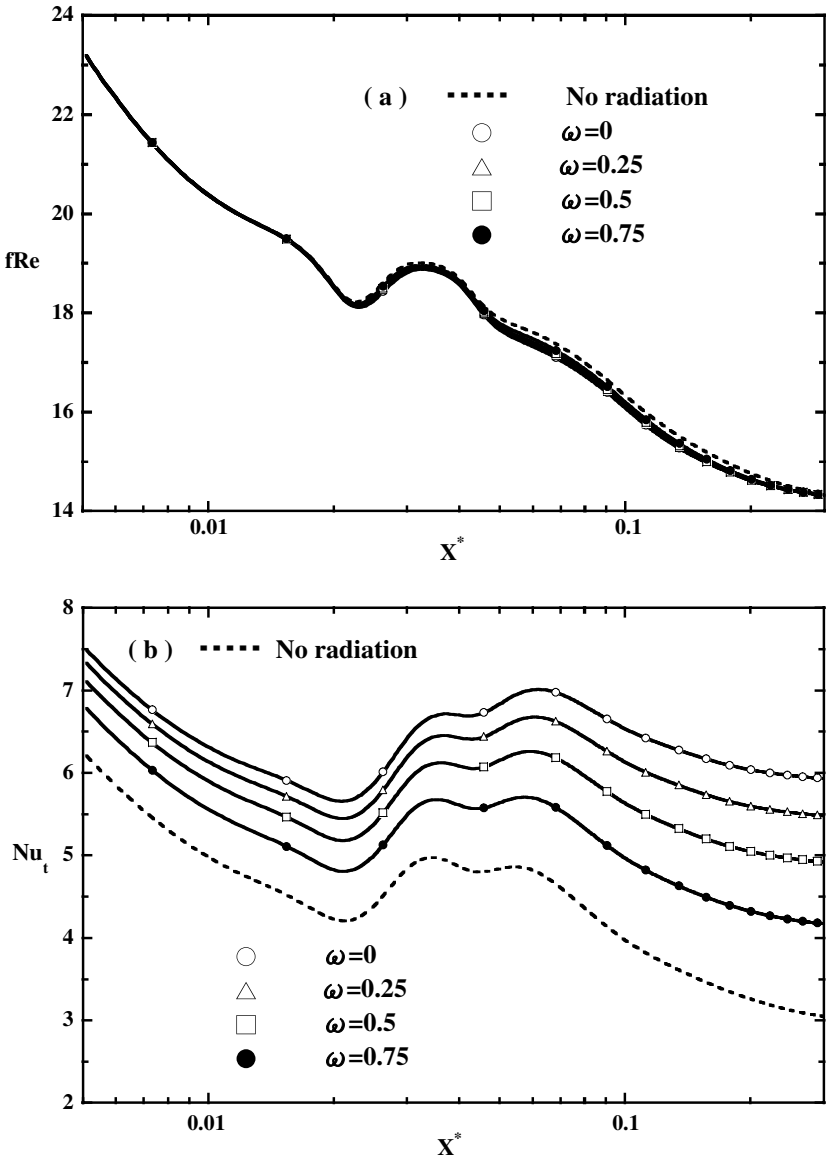

Fig. 10. Effect of ω on the axial distributions of fRe and Nu_t.

tration, the scattering is assumed to be isotropic. Fig. 10 presents the effects of single scattering albedo ω on the axial distributions of local fRe and Nu_t. The amount of energy that impinges upon the gray medium depends on the scattering albedo. When single scattering albedo ω approaches zero, the emission and absorption of the radiative energy within the medium dominate. But as the scattering albedo ω approaches unity, the scattering of the radiative heat transfer dominates. It is seen in Fig. 10a that when ω is 0, the local fRe is attenuated slightly due to the most radiation effects. In Fig. 10b, the local Nu_t is apparently raised with decreasing ω. For $\omega = 0$, Nu_t reaches its maximum value.

5. Conclusion

In this work, combined radiation and mixed convection heat transfer in rectangular ducts rotating in a parallel mode has been studied numerically. The vorticity-velocity method is successively employed to solve the three-dimensional parabolic governing equations. The radiative transfer equation was solved by the discrete ordinates method. The effects of the aspect ratio γ, rotational Reynolds number J, rotational Grashof number Gr_Ω, conduction-to-radiation parameter N_C and optical thickness τ on the fluid flow and heat transfer are examined in detail. What follow is a brief summary.

1. The rotational effects are more pronounced for a square duct ($\gamma = 1$) than rectangular ones.
2. The axial distributions of fRe and Nu_t are characterized by a drop near the inlet due to the entranced effect, but the decay is reduced by the onset of secondary flow.
3. The circumferentially averaged friction factor fRe and total Nusselt number are enhanced with increase of the rotational parameters J as well as Gr_Ω.
4. The total Nusselt number, Nu_t, are augmented by the radiation effects. On the other hand, the value of fRe is slightly reduced in the presence of radiation.
5. Radiation effects augment the Nu_t, and the extent of enhancement in Nu_t increases with a decrease (increase) in N_C or ω. Contrarily, the enhancement in Nu_t increases with an increase in τ or ε_w.

Acknowledgements

The financial support of this research by the National Science Council, ROC, under the Contract NSC93-2212-E211-011, is appreciated. Also, the financial support from Technology and Science Institute of Northern Taiwan is acknowledged.

References

[1] C.Y. Soong, W.M. Yan, Development of secondary flow and convective heat transfer in isothermal/iso-flux rectangular ducts rotating about a parallel axis, Int. J. Heat Mass Transfer 42 (1999) 497–510.
[2] W.D. Morris, Laminar convection in a heated vertical tube rotating about a parallel axis, J. Fluid Mech. 21 (1965) 453–464.
[3] J.E. Hart, Instability and secondary flow in a rotating channel flow, J. Fluid Mech. 45 (1971) 341–351.
[4] H. Ito, K. Nanbu, Flow in rotating straight pipes of circular cross section, J. Basic Eng. 93 (1971) 383–394.
[5] J. Moore, A wake and eddy in a rotating, radial flow passage. Part 1: experimental observations, J. Eng. Power 95 (1973) 205–212.
[6] J. Moore, A wake and eddy in a rotating, radial flow passage. Part 2: flow model, J. Eng. Power 95 (1973) 213–219.
[7] A.K. Majumdar, V.S. Pratap, D.B. Spalding, Numerical computation of flow in rotating ducts, J. Fluid Eng. 99 (1977) 148–153.
[8] C.G. Speziale, Numerical study of viscous flow in rotating rectangular ducts, J. Fluid Mech. 122 (1982) 251–271.
[9] C.G. Speziale, S. Thangam, Numerical study of secondary flows and roo-cell instabilities in rotating channel flow, J. Fluid Mech. 130 (1983) 377–395.
[10] C.G. Speziale, Numerical solution of rotating internal flows, Lectures Appl. Math. 22 (1985) 261–289.
[11] Y. Mori, T. Fukada, W. Nakayama, Convective heat transfer in a rotating radial circular pipe (2nd report), Int. J. Heat Mass Transfer 11 (1971) 1807–1824.
[12] V. Vidyanidhi, V.V.S. Suryanarayana, R. Chenchu, Analysis of steady fully developed heat transfer in a rotating straight pipe, J. Heat Transfer 99 (1977) 148–153.
[13] G.J. Hwang, T.C. Jen, Convective heat transfer in rotating isothermal ducts, Int. J. Heat Mass Transfer 33 (1990) 1817–1828.
[14] T.C. Jen, A.S. Lavine, G.J. Hwang, Simultaneously developing laminar convection in rotating isothermal square channels, Int. J. Heat Mass Transfer 35 (1992) 239–254.
[15] T.C. Jen, A.S. Lavine, Laminar heat transfer and fluid flow in the entrance region of a rotating duct with rectangular cross section: the effect of aspect ratio, J. Heat Transfer 114 (1992) 574–581.
[16] D. Skiadaressis, D.B. Spalding, Laminar heat transfer in a pipe rotating around a parallel axis, Report HRS/76123, Mechanical Engineering Department, Imperial College of Science and Technology, London, UK, 1976.
[17] M. Mahadeveppa, K.V.C. Rao, V.M.K. Sastri, Numerical study of laminar fully developed fluid flow and heat transfer in rectangular and elliptical ducts rotating about a parallel axis, Int. J. Heat Mass Transfer 39 (1996) 867–875.
[18] J.L. Woods, Heat transfer and flow resistance in a rotating duct system, Ph.D. Dissertation, University of Susses, Falmer, UK, 1975.
[19] A.R. Johnson, W.D. Morris, Pressure loss measurement in circular ducts which rotate about a parallel axis, in: Proceedings of the XIV ICHMT Symposium in Rotating Machinery, Dubrovnick, Yugoslavia, hemisphere Pub., Washington, USA, 1982, pp. 51–62.
[20] W.D. Morris, F.M. Dias, Turbulent heat transfer in a revolving square-sectioned tube, J. Mech. Eng. Sci 22 (1980) 95–101.
[21] A.R. Johnson, W.D. Morris, An experimental investigation into the effects of rotation on the isothermal flow resistance in circular tubes rotating about a parallel axis, Int. J. Heat Fluid Flow 13 (1992) 132–140.
[22] M. Mahadeveppa, K.V.C. Rao, V.M.K. Sastri, Experimental investigation for fluid flow and heat transfer in an elliptical duct rotating about a parallel axis, Exp. Heat Transfer 6 (1993) 97–109.
[23] S. Neti, A.S. Warnork, E.K. Levy, K.S. Kannan, Computation of laminar heat transfer in rotating rectangular ducts, ASME J. Heat Transfer 107 (1985) 575–582.
[24] E. Levy, S. Neti, G. Brown, F. Bayat, Laminar heat transfer and pressure drop in a rectangular duct rotating about a parallel axis, ASME J. Heat Transfer 108 (1986) 350–356.
[25] C.P. Tso, L.F. Lin, S.K.W. Tou, Numerical segregation of the effects of body forces in a rotating, differentially heated enclosure, Numer. Heat Transfer, Part A: Appl. 51 (2007) 85–107.

[26] M.P. King, M. Wilson, Numerical simulation of convective heat transfer in Rayleigh–Benard convection and a rotating annulus, Numer. Heat Transfer; Part A: Appl. 48 (2005) 529–545.
[27] J.C. Chawla, S.H. Chan, Spline collocation solution of combined radiation–convection in thermally developing flows with scattering, Numer. Heat Transfer 3 (1980) 47–65.
[28] F.H. Azad, M.F. Modest, Combined radiation and convection in absorbing, emitting and anisotropically scattering gas-particulate tube flow, Int. J. Heat Mass Transfer 24 (1981) 1681–1697.
[29] Y. Yender, M.N. Ozisik, Simultaneous radiation and forced convection in thermally developing turbulent flow through a parallel-plate channel, ASME J. Heat Transfer 108 (1986) 985–988.
[30] C.K. Krishnaprakas, K.B. Narayama, P. Dutta, Combined convective and radiative heat transfer in turbulent tube flow, J. Thermophys. Heat Transfer 13 (1999) 390–394.
[31] R.A. Shah, A.L. London, Laminar Flow Forced Convection in Ducts, Suppl. to Adv. Heat Transfer, Academic Press, New York, 1978, pp. 196–222.
[32] K. Ramakrishna, S.G. Rubin, P.K. Khosla, Laminar natural convection along vertical square ducts, Numer. Heat Transfer 5 (1982) 59–79.
[33] W.M. Yan, C.Y. Soong, Simultaneously developing mixed convection in radially rotating rectangular ducts, Int. J. Heat Mass Transfer 33 (1995) 665–677.
[34] W.A. Fiveland, Three-dimensional radiative heat transfer solution by the discrete-ordinates method, J. Thermophys. Heat Transfer 2 (1988) 309–316.
[35] T.Y. Kim, S.W. Baek, Analysis of combined conductive and radiative heat transfer in a two-dimensional rectangular enclosure using the discrete ordinates method, Int. J. Heat Mass Transfer 34 (1991) 2265–2273.
[36] M.F. Modest, Radiative Heat Transfer, McGraw-Hill, New York, 1993, pp. 541–571.
[37] B.G. Carlson, K.D. Lathrop, Transport theory: the method of discrete ordinates, in: H. Greenspan, C.N. Kelber, D. Okrent (Eds.), Computing Methods in Reactor Physics, Gordon & Breach Press, New York, 1968, pp. 165–266.